Stemness and Regenerative Potential of Corneal Stromal Stem Cells and Their Secretome After Long-Term Storage: Implications for Ocular Regeneration

Ajay Kumar,[1] Yi Xu,[1] Enzhi Yang,[1] and Yiqin Du[1–4]

[1]Department of Ophthalmology, University of Pittsburgh, Pittsburgh, Pennsylvania, United States
[2]Department of Developmental Biology, University of Pittsburgh, Pittsburgh, Pennsylvania, United States
[3]McGowan Institute for Regenerative Medicine, University of Pittsburgh, Pittsburgh, Pennsylvania, United States
[4]Shanghai Oriental Hospital, Tongji University, Shanghai, China

Correspondence: Yiqin Du, 910 Eye and Ear Institute, 203 Lothrop Street, Pittsburgh, PA 15213, USA; duy@upmc.edu

Submitted: January 8, 2018
Accepted: June 14, 2018

Citation: Kumar A, Xu Y, Yang E, Du Y. Stemness and regenerative potential of corneal stromal stem cells and their secretome after long-term storage: implications for ocular regeneration. *Invest Ophthalmol Vis Sci*. 2018;59:3728–3738. https://doi.org/10.1167/iovs.18-23824

Purpose. To assess the stemness and regenerative potential of cryopreserved corneal stromal stem cells (cryo-CSSCs) after long-term storage. We also used the secretome from these cells to observe the effect on wound-healing capacity of corneal fibroblasts and on the expression of fibrotic markers during wound healing.

Methods. CSSCs were obtained from three donors and stored in liquid nitrogen for approximately 10 years. Post thaw, cryo-CSSCs were characterized for stemness using phenotypic and genotypic markers along with colony-forming efficiency and three-dimensional spheroid formation. Multilineage differentiation was observed by differentiation into osteocytes, adipocytes, neural cells, and keratocytes. Secretome was harvested by culturing cryo-CSSCs in log phase. Wound-healing capacity was observed by live-cell time-lapse microscopy. Statistical analysis was done using 1-way ANOVA and Tukey posttest.

Results. CSSCs displayed good viability post thaw and showed >90% expression of stem cell markers CD90, CD73, CD105, STRO1, and CD166. cryo-CSSCs also expressed stem cell genes OCT4, KLF4, and ABCG2, and could also form colonies and three-dimensional spheroids. Multipotency assessment showed that all three cryo-CSSCs could differentiate into osteocytes, adipocytes, neural cells, as shown by β-III tubulin and neurofilament antibody staining and corneal keratocytes as observed by staining for Kera C, J19, and collagen V antibodies. The secretome derived from these three populations could promote the wound healing of corneal fibroblasts and reduce the expression of fibrotic markers SPARC and fibronectin.

Conclusions. CSSCs maintained their stemness and multipotency after long-term storage, and secretome derived from these cells can be of paramount importance for corneal regeneration and prevention of fibrosis.

Keywords: corneal stromal stem cells, regeneration, cryopreservation, multipotency, secretome

Regenerative medicine has progressed a lot in past decade with stem cell therapy (SCT) being used for a number of devastating disease like Parkinson's,[1] Alzheimer's,[2] stroke,[3] spinal cord injury,[4] and heart disorders.[5] In ocular disorders, stem cells have been successfully used in ocular surface reconstruction[6] and also for inducing tolerance while doing allograft limbal transplants.[7] Some of the diseases, like optic and retinal neuropathies, acute onset of myocardial infarction, and stroke, would require immediate transplantation of stem cells for fast therapeutic recovery. The application of stem cells in hundreds of clinical trials would require these cells to be cryopreserved to meet the high dose demand at the time of treatment, which is one of the main goals for "off-the-shelf" SCT. However, there are no studies available about the multipotency and stemness of stem cells after long-term cryopreservation (>10 years). Harsh conditions of cryopreservation can alter the biological properties of stem cells, compromising their use for downstream clinical and research-based application.[8] There are vast studies available in the literature with contrasting findings.[9] An important study by Moll et al.[10] reported that continuously passaged early-passage fresh mesenchymal stem cells (MSCs) showed a better therapeutic outcome in patients with acute graft versus host disease (GvHD) as compared to cryopreserved MSCs when transplanted as intravenous injections. In another study, Francois et al.[11] showed that cell viability of freshly thawed MSCs was significantly very low as compared with cells that were maintained continuously in culture for more than 1 week. However, Luetzkendorf and colleagues[12] reported that the proliferation, viability, and immunosuppressive properties of MSCs remain intact after cryopreservation. Similarly, Katayama et al.[13] showed that peripheral blood stem cells maintain their viability even after 5 years of long-term cryopreservation. Gramlich et al.[14] reported that MSCs maintain their potency in retinal ischemia model after 7 to 30 days of cryopreservation. Working together with the Funderburgh group at the University of Pittsburgh, we first characterized the corneal stromal stem cells (CSSCs) as a rare population in human corneal stroma.[15]

CSSCs have potency of multilineage differentiation.[15] CSSCs have been used in various applications related to ocular regeneration, like prevention and reduction of corneal scarring,[16–18] and also in generation of corneal tissues resembling in structure with human cornea.[19–23] In contrast, corneal fibroblasts, unlike CSSCs, do not have regenerative effects and rather induce fibrotic and inflammatory response in vivo.[18,24] The CSSCs can be easily obtained by biopsy from the corneal limbus,[16] and there can be a possibility of enhanced therapeutic benefit of CSSCs in corneal regeneration because these cells are natural progenitors of corneal keratocytes and are derived from neural crest. Thus, they are also an attractive candidate for autologous SCT in patients. However, there is no evidence available to date about the regenerative potential of CSSCs or any other ocular stem cells after long-term cryopreservation.

The ability of stem cells to repopulate, differentiate, and induce a therapeutic benefit largely depends on host microenvironment. There are limited studies available about whether the trophic factor support from host is sufficient to maintain the viability of transplanted stem cells.[25] Recently, there have been a number of studies in which trophic factors derived from stem cells, collectively known as secretome, have been beneficial in a range of diseased conditions, including improvement in cardiac functions,[26] promoting wound healing,[27] and recovery from cognitive impairment.[28] Stem cell secretome has been increasingly used now as a potential drug candidate holding immense hope for future regenerative medicine.[29–31] Fibrosis, a response of the tissue to injuries, is a serious concern in many diseases, including corneal scarring after injury or infection leading to excessive extracellular matrix (ECM) deposition and vision reduction and vision loss over time.[32,33] Because there is sparse literature available about the regenerative potential of secretome on corneal wound healing and fibrosis, we sought to investigate the effect of CSSC-derived secretome in this context. In this study, we investigate for the first time, the multipotency and stemness of CSSCs after long-term cryopreservation and efficacy of secretome derived from these stem cells in corneal wound healing and effect on fibrosis.

Materials and Methods

Thawing and Cell Culture

CSSCs were isolated from corneas of three donors aged 15 to 45 years old, as described in Supplementary Table S1 and cultured in a stem cell growth medium (SCGM)[15] consisting of Dulbecco's modified Eagle's medium (DMEM) low glucose, MCDB-201, insulin-transferrin-selenious acid supplement (Sigma-Aldrich, St. Louis, MO, USA), gentamicin, albumin, fetal bovine serum (FBS) (2%) (Gibco, Gaithersburg, MD, USA), ascorbic acid-2-phosphate, dexamethasone, platelet-derived growth factor, epidermal growth factor, and antibiotics penicillin/streptomycin (Gibco). Cells were cryopreserved in liquid nitrogen using 70% DMEM/HAMs F12, 20% FBS, and 10% dimethyl sulfoxide (DMSO) for 10 years or more. After 10 years, CSSCs were quickly thawed using water bath maintained at 37°C and cultured in SCGM. TrypLE express (Gibco) was used for cell detachment and further upscale. Cells were routinely observed under bright field inverted microscope (Nikon Eclipse TS100; Melville, NY, USA) and medium was changed every third day.

MTT Assay

Per well of 96-well plates, 5×10^3 CSSCs were cultured for 24 hours and then incubated with SCGM for 48 hours. MTT reagent was added to cells 4 hours before completion of incubation period and the resulted formazan crystals were dissolved using DMSO by subsequent cell lysis. For MTT assay, the absorbance (570 nm) and reference (600 nm) wavelengths were used in a microplate reader (Synergy 2; BioTek, Winooski, VT, USA) to measure absorbance and the final inferences were drawn by subtracting the reference reads from measurement reads. The percentage of cell viability was then calculated using the formula, (OD sample)/(OD control) × 100. HC111 was taken as control for comparison of cell viability with other cell types and cell viability was considered as 100% for this.

Calcein/Hoechst Staining

Cells were cultured for 24 to 48 hours in six-well culture dishes at a density of 5×10^4 cells per well in SCGM at 37°C/5% CO_2 incubator. Cells were stained with 0.001× Calcein red Orange (Invitrogen, Carlsbad, CA, USA) and 0.0005× Hoechst 33342 for 10 minutes. Proper wash of PBS (pH 7) was given before and after staining. Cells were photographed using inverted fluorescence microscope (Nikon Eclipse TE 2000-E) using excitation/emission of 577/590 nm for Calcein and 361/497 for Hoechst 33342.

Cell Proliferation Assay

In 96-well plates, 5×10^3 CSSCs were plated in hexapulicates. Cells were cultured for 24 hours in SCGM and then incubated with 10% Alamar blue solution (Bio-Rad, Hercules, CA, USA). Absorbance of the samples was read after an interval of every 4 hours for 24 hours at 570 nm by taking 600 nm as reference wavelength using a microplate reader. Reference wavelength was subtracted from measurement wavelength to drive final optical density. Temporal reduction of Alamar blue to red stain by metabolically active cells was recorded and reference wavelength was subtracted from measurement wavelength to calculate the final cell proliferation for each cell type. Optical density measurements for each cell type were extrapolated to calculate the cell proliferation cells using HC111 as control.

Flow Cytometry

CSSCs were cultured in 75 cm^2 flasks for 48 to 72 hours and cells were trypsinized upon reaching 70% to 80% confluence. CSSCs were incubated with 1% BSA for 30 minutes to block the nonspecific sites after PBS wash. These cells were then incubated with different antibodies conjugated directly with different fluorochromes for 30 minutes on ice in the dark (Supplementary Table S2). Proper negative, isotype, and compensation controls were run for each fluorochrome. The unstained cells served as negative control to eliminate any background fluorescence generated by cells. After incubation, approximately 5×10^4 cells were acquired per cell type for each antibody in triplicates on BD FACSAria run with FACSDIVA software (BD Biosciences, San Jose, CA, USA). Analysis was done using FlowJo_V10 flow cytometry analysis software (FlowJo, Ashland, OR, USA).

Real-Time PCR Analysis

Cells were cultured to 80% confluence in SCGM and then lysed using RLT buffer (Qiagen, Valencia, CA, USA) after a single PBS wash. RNA was extracted from cells using RNeasy Mini Kit (Qiagen) by following the instructions given in the kit. cDNA was reverse transcribed from approximately 500 ng RNA using a high-capacity cDNA reverse transcription kit (Applied Biosystems, Foster City, CA, USA); 18S was used as housekeeping control. Real-time PCR reaction was performed on StepOne

Investigative Ophthalmology & Visual Science

plus 7700 instrument (Applied Biosystems). The primer sequence for 18S, OCT4, KLF4, ABCG2, and Nestin is given in Supplementary Table S3.

Colony-Formation Assay

Per well of six-well plates, 1000 CSSCs for each cell type were plated at least in triplicate in SCGM. These cells were allowed to form colonies for 7 days. After 7 days, cell colonies were stained with 0.01% crystal violet for 30 minutes and counted under microscope after washing. Colonies were photographed using EVOS XL core microscope (Life Technologies, Carlsbad, CA, USA). Crystal violet was extracted from colonies after incubation with 100% isopropanol in chemical hood for 10 minutes and absorbance of extracted crystal violet was read at 570 nm using a plate reader.

Spheroid Formation Assay

A total of 1000 CSSCs were plated per well of ultra-low attachment six-well plates in SCGM. Spheroids formed by CSSCs were captured on different days using phase-contrast on a Nikon Eclipse TE 200 inverted fluorescence microscope (Nikon, Tokyo, Japan). Area of spheroids was measured using NIS elements software (Nikon). At least 10 images per cell type were used for area quantification.

Osteogenic Differentiation

A total of 1×10^4 cells were seeded per well of 12-well plates and cultured until 70% to 80% confluence. After that, cells were induced for osteocyte differentiation using osteogenic differentiation medium (Gibco) with osteogenic differentiation supplement for the duration of 21 days. At the end of differentiation, cells were characterized for calcium deposition using Alizarin red solution (EMD Millipore, Bedford, MA, USA) for 30 minutes. Cells were washed with ddH_2O and photographed using a bright-field microscope (EVOS XL Core; Life Technologies). Alizarin red was extracted using cetylpyridinium chloride (CPC) buffer (pH 7; Sigma-Aldrich) by incubating stained cells with buffer for 1 to 2 hours on continuous shaking. For quantification of osteogenic differentiation, measurement wavelength for absorbance was 570 nm. The values obtained as optical density measurements were plotted between control and respective differentiated cells for all three CSSCs.

Adipogenic Differentiation

A total of 1×10^4 cells were seeded as described for osteogenic differentiation and induced for adipogenic differentiation using adipogenic differentiation media (Gibco) for a duration of 16 days. After differentiation, cells were stained for Oil Red O (Sigma-Aldrich), which binds with oil granules deposited in differentiated adipocytes. Parallel undifferentiated cells served as controls. Cells were photographed using an EVOS XL core light microscope.

Neural Differentiation

A total of 1×10^4 CSSCs were plated per well of 12-well plates and cultured in SCGM until 60% to 70% confluence. Cells were differentiated to neurons using neurobasal medium supplemented with epidermal growth factor (20 ng/mL), bFGF (20 ng/mL), B27 supplement (1:50), N2 supplement (1:100), and 2% knockout serum replacement for 39 to 41 days. Medium was replenished every fourth day. At the end of neural differentiation, cells were characterized by β-III tubulin and neurofilament antibody staining. Parallel control cells were cultured without any differentiation supplement and stained with neural antibodies.

Keratocyte Differentiation

Keratocyte differentiation was followed using the procedures described previously[20] with subtle modifications. In brief, 3×10^5 CSSCs per cell type were maintained in 15-mL Falcon tubes and cultured for 3 days in SCGM in the form of pellets. The medium was then changed to keratocyte differentiation medium (KDM) containing advanced-minimal essential medium, ascorbic acid 2-phosphate (A-2-P, 0.5 mM), and FGF (10 ng/mL). Cell pellets were cultured in KDM for 3 weeks. Medium was replenished every fourth day. At the end of differentiation, cells were fixed and characterized with different antibodies pertaining to keratocyte differentiation.

Immunofluorescent Staining

Cells were fixed using neutral buffered formalin after brief PBS wash. Cell permeabilization was achieved by treating them with 0.1% Triton X-100 for 10 minutes. The nonspecific sites were blocked by incubating cells with 1% BSA for 0.5 hour. Cells were then incubated with respective differentiation antibodies overnight at 4°C: βIII tubulin (1:100; Invitrogen) and neurofilament (1:100; EMD Millipore) for neural differentiation; Kera C to keratocan (1:100; a gift from Chia-Yang Liu, PhD, Indiana University), J19 to keratan sulfate (1:100; a gift from James Funderburgh, PhD, University of Pittsburgh) and collagen V (1:100; EMD Millipore) for keratocyte differentiation. Next day, cells were incubated with secondary antibodies, such as donkey-anti-goat-488, donkey-anti-rabbit-546, and donkey-anti-mouse-633. DAPI (4′,6-diamidino-2-phenylindole, dihydrochloride) was used as nuclear stain. Cells were photographed using a laser scanning confocal microscope (IX81; Olympus, Tokyo, Japan). The color histogram plugin of ImageJ (http://imagej.nih.gov/ij/; provided in the public domain by the National Institutes of Health, Bethesda, MD, USA) was used to quantify fluorescence intensity of the image as a whole, and on an average the intensity was calculated for at least three images. To validate this, intensity of individual cells was also measured using NIS elements software package provided with the inverted fluorescent microscope (Nikon Eclipse TE 2000-E) and similar results were obtained.

Secretome Harvesting

Cells were grown to 60% to 70% confluence and then incubated with SCGM in log phase for 48 to 72 hours. Conditioned medium was harvested from cells, centrifuged for 5 minutes to remove any cell debris, and then stored at −80°C until further use. For all cell-based experiments, this conditioned medium was used in 1:1 dilution with culture media.

Wound-Healing Assay and Time-Lapse Microscopy

For wound-healing assay, 1×10^5 corneal fibroblasts were plated per well of a six-well plate. These cells were allowed to grow to 80% to 90% confluence. Wound was created using a 100-μL micro tip in vertical position. Cells were then incubated with secretome and control medium for 9 to 12 hours and photographed using live-cell time-lapse microscopy (Nikon Eclipse Ti). Multiple-stage positions were set for automated image capturing at defined time intervals. Analysis of wound healing was done using ImageJ software.

Investigative Ophthalmology & Visual Science

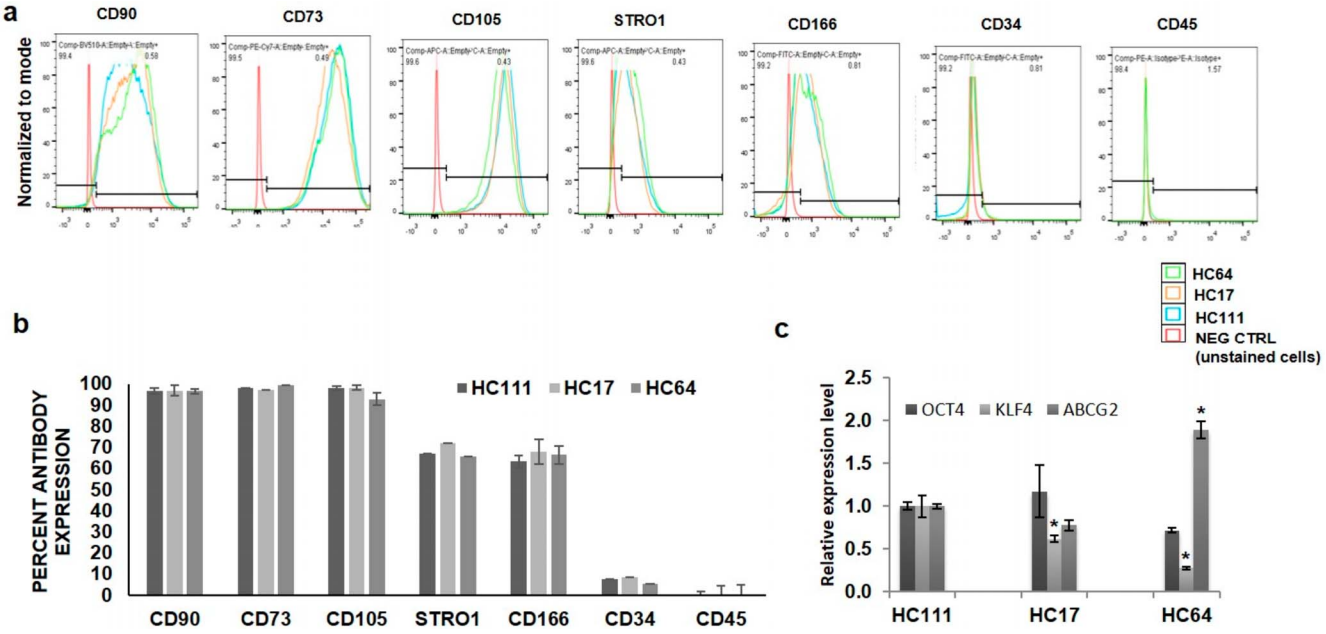

Figure 1. Characterization of cell stemness. (**a**) *Histograms* showing the percentage of three CSSC populations of various stemness markers, endothelial and hematopoietic markers. (**b**) *Bar diagram* showing the comparative expression of various markers in CSSCs. (**c**) Real-time expression profiling for various stemness genes in three CSSC populations. $^{*}P < 0.05$, $^{**}P < 0.001$, $^{***}P < 0.0001$.

Statistical Analysis

The values given are represented as mean ± SD. All experiments were performed at least in triplicate. Statistical analysis was done with 1-way ANOVA using SAS statistical analysis software (version 9.4; SAS Institute Inc., Cary, NC, USA). The *P* values for the multiple comparisons were adjusted using the Tukey method. Statistical significance was considered at $P < 0.05$.

Results

Assessment of Cell Viability and Characterization of Stemness in Cryo-CSSCs Post Thaw

We have previously reported the isolation and characterization of multipotent stem cells from human cornea along with their potency for multilineage differentiation.[23] Three cryopreserved CSSCs were thawed after 10 years of cryopreservation and cultured. Supplementary Figure S1a shows the morphology of cells under phase-contrast microscope after 24 hours of culture. Cell viability assessment by Calcein/Hoechst staining showed that all cells were fully viable after thawing (Supplementary Fig. S1b). Quantitative analysis of cell viability by MTT assay showed no significant differences in cell viability among different CSSC populations (Supplementary Fig. S1c). Assessment of cell proliferation capacity of these cells for 24 hours by Alamar blue cell proliferation assay (Supplementary Fig. S1d) showed no significant difference in the proliferation potential of three CSSCs. Characterization of stemness in thawed CSSCs was done by flow cytometry and quantitative PCR (qPCR) for various positive stem cell surface markers. Flow cytometry analysis showed that all three CSSCs expressed stem cell markers with CD90, CD73, and CD105 >90% positivity and CD166 and STRO1 >60% positivity. On the other hand, the expression of negative stem cell markers, such as CD34 and CD45, was <5% (Figs. 1a, 1b). qPCR analysis showed the positive expression of stem cell genes OCT4, KLF4, and ABCG2 in all three populations; however, the expression of ABCG2 was a little bit higher and KLF4 was lower in HC64 as compared with HC111 and HC17 (Fig. 1c).

Colony Formation Efficiency (CFE) and Spheroid Formation Ability of Cryo-CSSCs

All CSSCs were able to arrange themselves into spherical colonies after defined time interval, which reflected the colony-forming potential of single cells from all three CSSCs. The colonies from all three CSSCs were stained with crystal violet after fixation (Fig. 2a). The colony count from three CSSC types showed a significantly higher CFE of HC111 (23.3 ± 4.8) and HC17 (25.5 ± 2.5) as compared with HC64 (7.1 ± 2.1) (Fig. 2b). These results were further validated by extracting the crystal violet from stained colonies and reading the absorbance from extracted crystal violet. Optical density results showed significantly higher CFE of HC111 (0.87 ± 0.2) and HC17 (0.75 ± 0.05) as compared with HC64 (0.58 ± 0.05) (Fig. 2c). CSSCs were also assessed for their tendency to form three-dimensional spheroids in suspension culture. All three CSSCs were observed to form small ball-like spheroids at the third day of seeding, which were increased in size in all three CSSCs with time. The temporal increase in spheroid size with time is shown in Figure 3a. However, the size of spheroids was larger in HC111 (257.4 μm^2) and HC17 (256.8 μm^2) in comparison with HC64 (188.1 μm^2) by day 7, which was further increased to 300.5 μm^2 for HC111 but was reduced for HC17 (195.9 μm^2) to that of almost the same size of HC64 (201 μm^2) by day 15 (Fig. 3b). Calcein/Hoechst staining for the cell viability assessment of spheroids showed that spheroids from all three CSSCs were fully viable even after 15 days of suspension culture (Fig. 3c). We also observed the expression of stem cell genes OCT4, KLF4, and ABCG2 in these spheroids at day 15, and found that spheroids from all three CSSC populations expressed the above three genes (Fig. 3d).

Investigative Ophthalmology & Visual Science

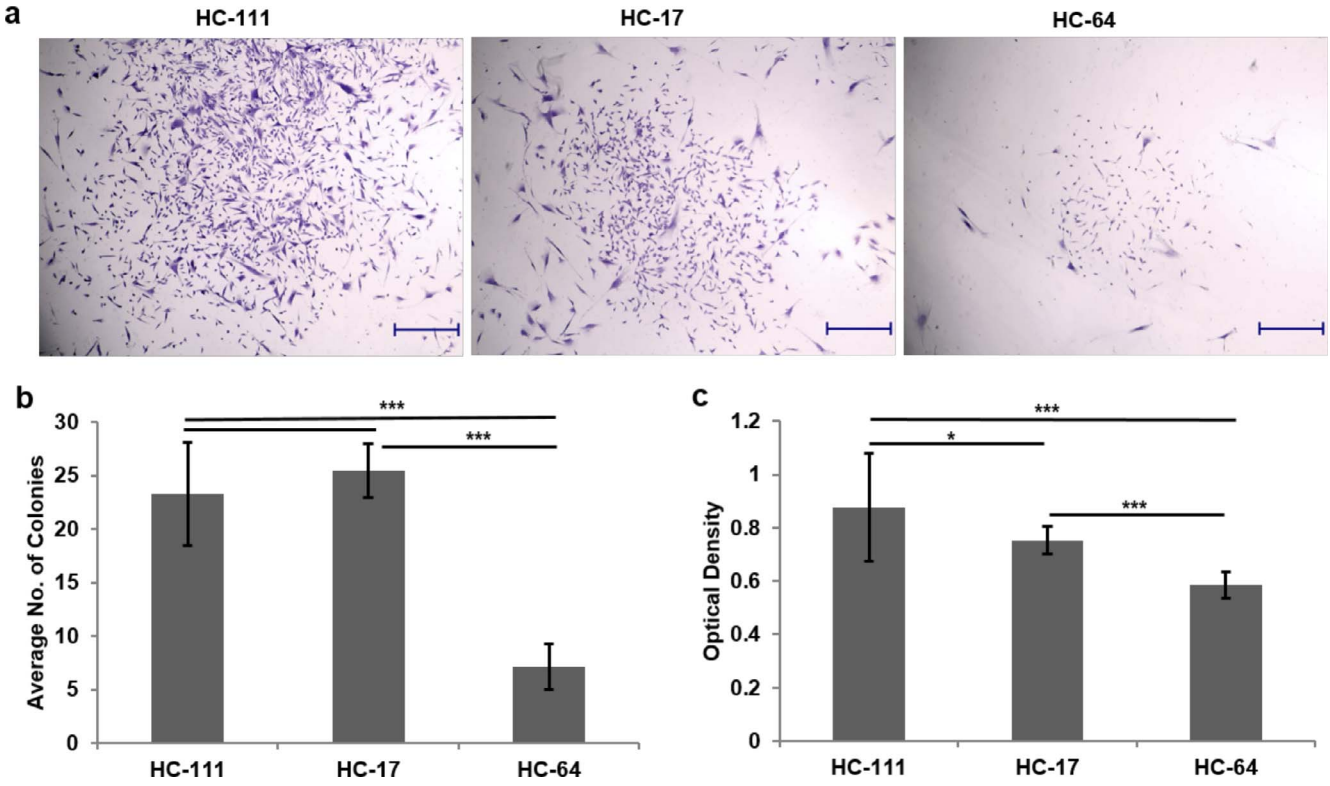

Figure 2. Colony formation unit assay. (**a**) Stem cell colonies established after 7 days of culture. *Scale bar*: 500 μm. (**b**) *Bar diagram* showing the comparison of colony-forming efficiency of various CSSCs. (**c**) Measurement of crystal violet (CV) extracted from stained colonies. $^{*}P < 0.05$, $^{**}P < 0.001$, $^{***}P < 0.0001$.

Osteogenic/Adipogenic Differentiation Capacity of Cryo-CSSCs

Multipotency of CSSCs post thaw was evaluated by differentiating them into osteocytes, adipocytes, neural cells, and keratocytes. Tendency of CSSCs to differentiate into osteocytes was evaluated based on calcium granule deposition when cultured in osteogenic differentiation medium and qPCR for bone sialo protein (BSP) and osteocalcin. All three CSSCs showed the deposition of calcium granules that were stained positive for Alizarin red (Fig. 4a). Extraction of Alizarin red was performed with the help of CPC buffer to compare the degree of osteogenic differentiation, and we observed a significant increase in all CSSCs post osteogenic differentiation as compared with uninduced control. Comparison of osteogenic differentiation among three populations showed that HC17 (0.5 ± 0.05) and HC64 (0.35 ± 0.12) displayed higher osteogenic potential as compared with HC111 (0.18 ± 0.03) (Fig. 4b). qPCR analysis showed that BSP was increased significantly after osteogenic differentiation in HC111 and HC17, whereas HC64 displayed a significantly increased expression of osteocalcin post differentiation (Figs. 4c, 4d). It is worth mentioning that BSP was highest in HC17, which was in accordance with results obtained by Alizarin red staining.

Adipogenic differentiation was assessed based on uptake of Oil Red O stain by oil droplets that accumulate after adipogenic differentiation in adipocytes and qPCR for leptin. However, in contrast to osteogenic differentiation, we observed a higher adipogenic potential of HC111 and HC17 as compared with HC64 (Supplementary Fig. S2a). qPCR analysis confirmed these results where there was a significant increase in leptin after adipogenic differentiation and it was found to be highest in HC111 (Supplementary Fig. S2b).

Potential of Cryo-CSSCs to Differentiate into Neural Cells

Neural differentiation of the CSSCs was achieved by a synergistic application of neural induction medium and differentiation supplements. Neural differentiation was evaluated by immunofluorescence staining for neural antibodies β-III Tubulin and neurofilament (NF) and qPCR for Nestin and NF. All three CSSCs were observed to differentiate into neural cells with long axons. Post differentiation, cells from all three CSSCs showed positive staining for both β-III Tubulin and NF, whereas no antibody staining could be detected in control, undifferentiated cells (Figs. 5a, 5c). Comparison of fluorescence intensity for both antibodies showed a significantly high fluorescence intensity of β-III Tubulin in neural differentiated HC111 and HC17 (HC111-dif and HC17-dif) as compared with HC64 (HC64-dif) (Fig. 5b). However, the comparative evaluation of fluorescence intensity for NF showed no significant difference among three differentiated CSSC populations (Fig. 5d). qPCR analysis for expression of Nestin showed that CSSCs expressed Nestin at both control and differentiated level; however, a statistically significant elevated expression of Nestin was observed after differentiation for both HC111 and HC17, but no increased expression in case of HC64 (Fig. 5e). qPCR analysis for NF showed a significant increase in NF expression post neural differentiation in all three CSSCs (Fig. 5f).

Cryo-CSSCs Hold the Capacity to Differentiate Into Corneal Keratocytes

To explore the application of cryopreserved CSSCs for corneal regeneration, we assessed the differentiation potential of these cells into corneal keratocytes. This differentiation was achieved for culturing the cells in KDM for 3 weeks as cell

Investigative Ophthalmology & Visual Science

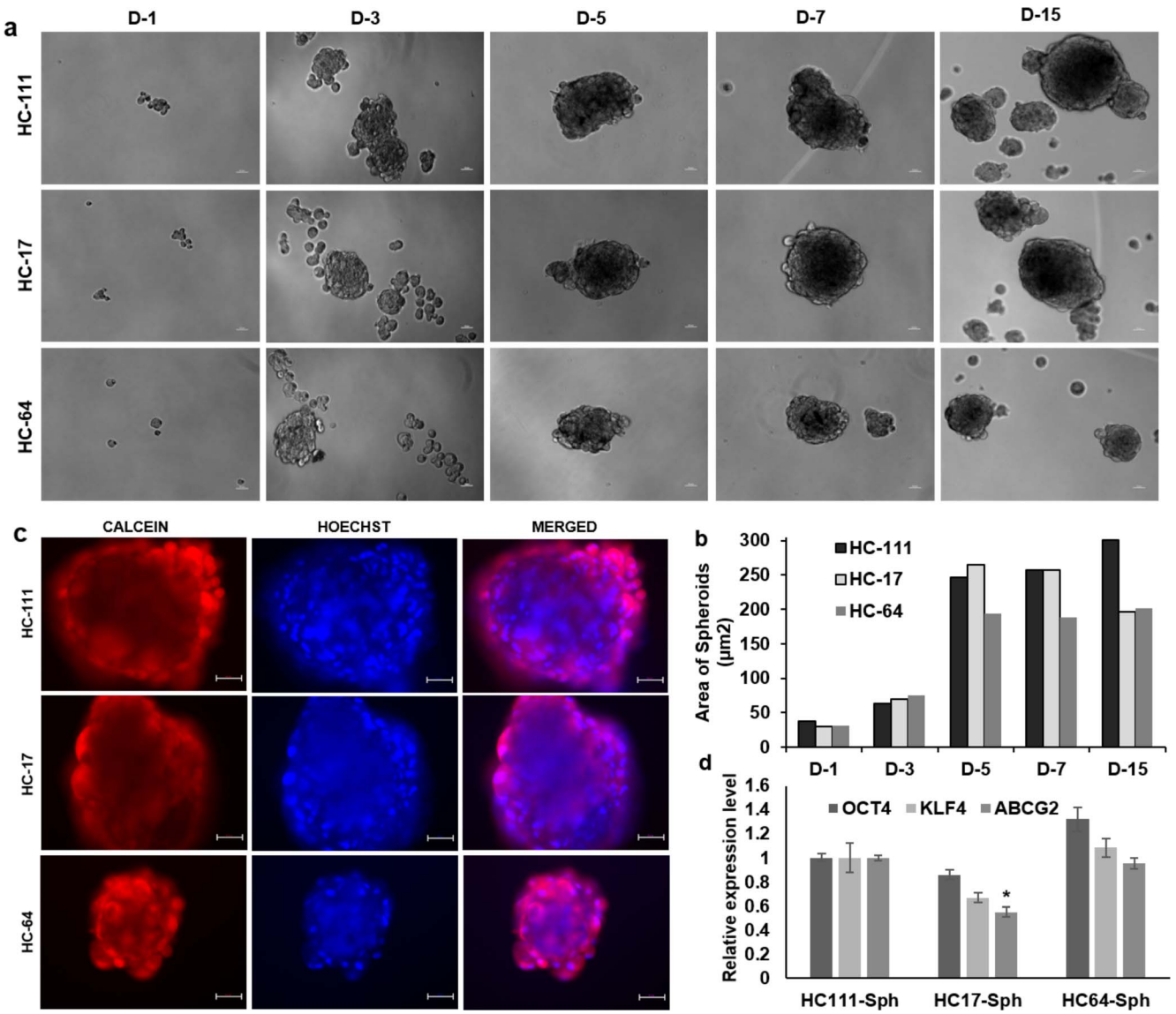

Figure 3. Spheroid formation. (**a**) Temporal phase-contrast images of spheroids formed at various time intervals by different CSSCs. *Scale bar*: 50 µm. (**b**) *Bar diagram* showing the comparison of spheroid size formed at various days (D1–D15). (**c**) Calcein/Hoechst staining of spheroids at D15 for assessment of spheroid viability. *Scale bar*: 50 µm. (**d**) Real-time PCR analysis for expression of various stemness genes in spheroids derived from different CSSC populations. $^{*}P < 0.05$, $^{**}P < 0.001$, $^{***}P < 0.0001$.

pellets. We observed that post differentiation, all three CSSC populations secreted keratocyte-specific ECM components keratocan (recognized by Kera C antibody) and keratan sulfate (recognized by J19 antibody staining) as well as collagen V (Fig. 6). The isotype control for all three secondary antibodies was used to stain the differentiated keratocyte pellet to exclude any possibility of nonspecific staining. It may be noted that there was no significant difference in the mean fluorescence intensity of Kera C among differentiated keratocytes from three CSSCs; however, J19 was significantly lower in HC17 as compared with other CSSCs, whereas collagen V showed the highest fluorescent intensity in HC64 (Figs. 6b–d).

Regenerative Potential of Secretome Derived From Cryo-CSSCs on Corneal Fibroblasts and Fibrosis

The tendency of these cells to make corneal keratocytes prompted us to assess the regenerative effect of secretome derived from these cells in promoting the wound-healing capacity of corneal fibroblasts and also the effect on fibrosis during corneal wound healing. We observed that secretome from HC64 could significantly increase the wound-healing potential of corneal fibroblasts after 6 to 9 hours of incubation, whereas secretome derived from HC111 and HC17 did not increase the wound-healing capacity of corneal fibroblasts to a significant level (Figs. 7a, 7b). The secretome from HC64 was able to decrease the expression of fibronectin and SPARC to a significant level. Secretome derived from HC111 and HC17 could significantly reduce the expression of fibronectin (Fig. 7c). The connective tissue growth factor (CTGF) levels were found to be unaltered in corneal fibroblasts after treatment with secretome derived from any of the CSSCs.

Discussion

Our study showed that CSSCs derived from all three cultures were able to maintain their viability post thaw even after 10

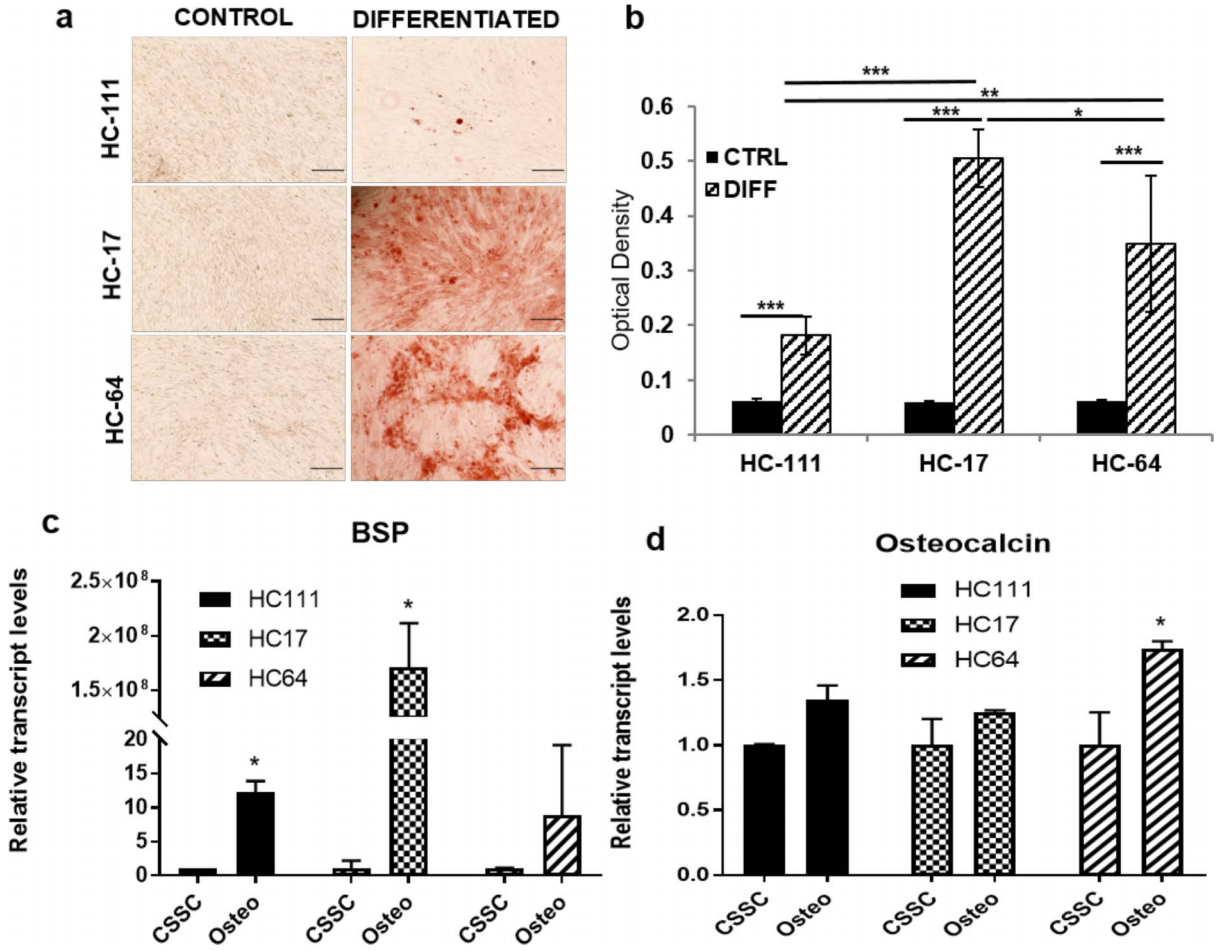

Figure 4. Osteogenic differentiation. (**a**) Light microscopy images for Alizarin red–stained cells at control and differentiation level. *Scale bar*: 200 µm. (**b**) *Bar diagram* depicting the comparative differentiation capacity after Alizarin red extraction. (**c**, **d**) *Bar diagram* showing comparison of gene expression for BSP and osteocalcin, respectively, in control and differentiated CSSCs. $^{*}P < 0.05$, $^{**}P < 0.001$, $^{***}P < 0.0001$.

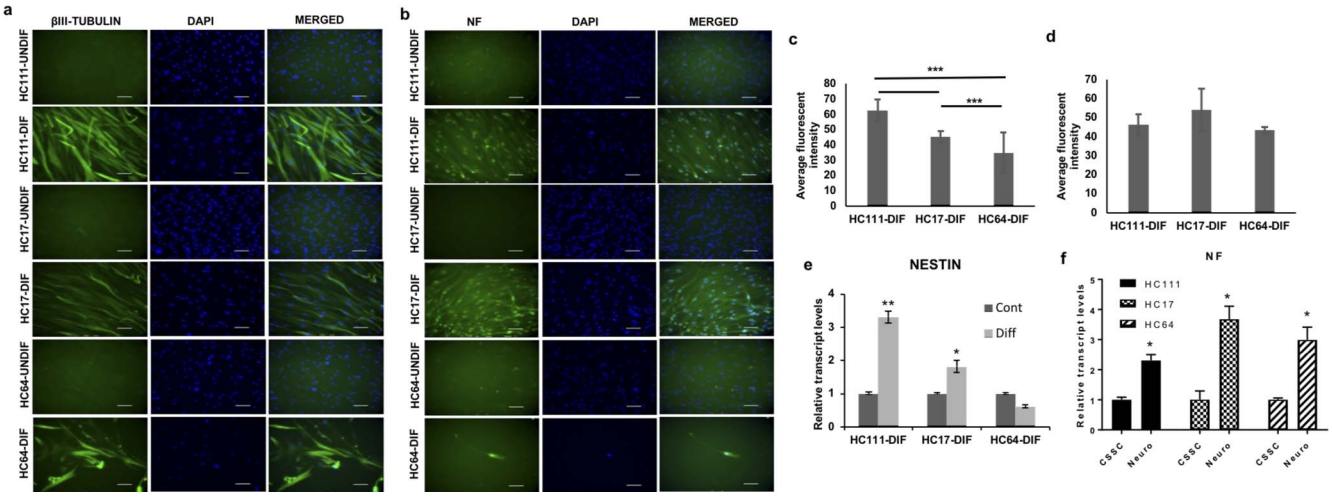

Figure 5. Neural differentiation. (**a**) *Fluorescent microscopic images* for βIII-Tubulin pre/post neural differentiation. (**b**) *Fluorescent images* showing expression of neurofilament (NFM) before/after neural differentiation. *Scale bar*: 50 µm. (**c**, **d**) *Bar diagram* showing the comparison of average fluorescent intensity for βIII-Tubulin and NFM antibody in different CSSC populations. (**e**, **f**) Real-time PCR expression analysis of Nestin and NFM, respectively, pre/post differentiation in different CSSCs. $^{*}P < 0.05$, $^{**}P < 0.001$, $^{***}P < 0.0001$.

Investigative Ophthalmology & Visual Science

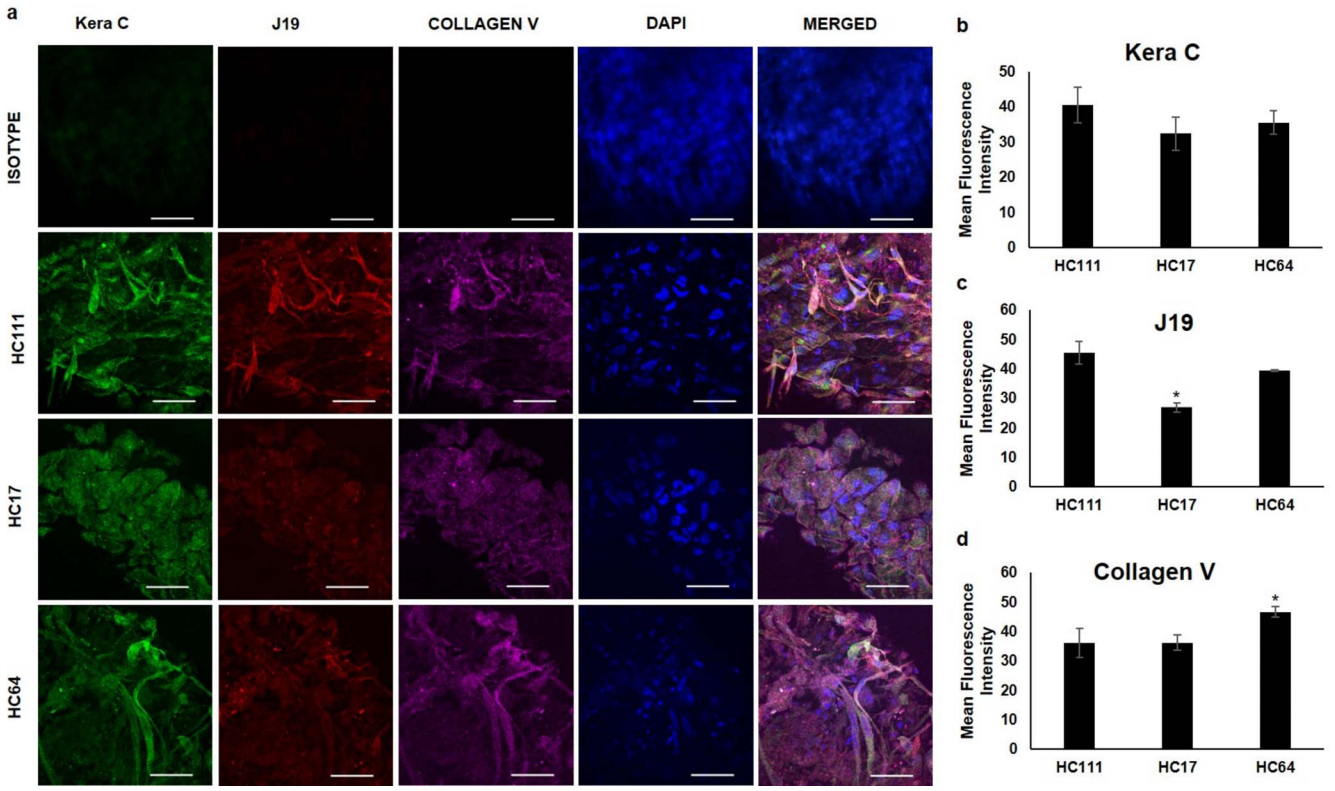

Figure 6. Keratocyte differentiation of CSSCs. (**a**) *Fluorescence microscopic images* of three-dimensional keratocyte spheroids formed post differentiation for various keratocyte proteins Kera C (*green*), J19 (*red*), and Collagen V (*purple*). DAPI was used as a nuclear stain. Isotype control for all three antibodies was used to avoid the possibility of nonspecific staining. *Scale bar*: 50 μm. (**b–d**) *Bar diagrams* showing quantification of mean fluorescence intensity for Kera C, J19, and Collagen V, respectively, in differentiated keratocytes from three corneal stem cells. $^{*}P < 0.05$.

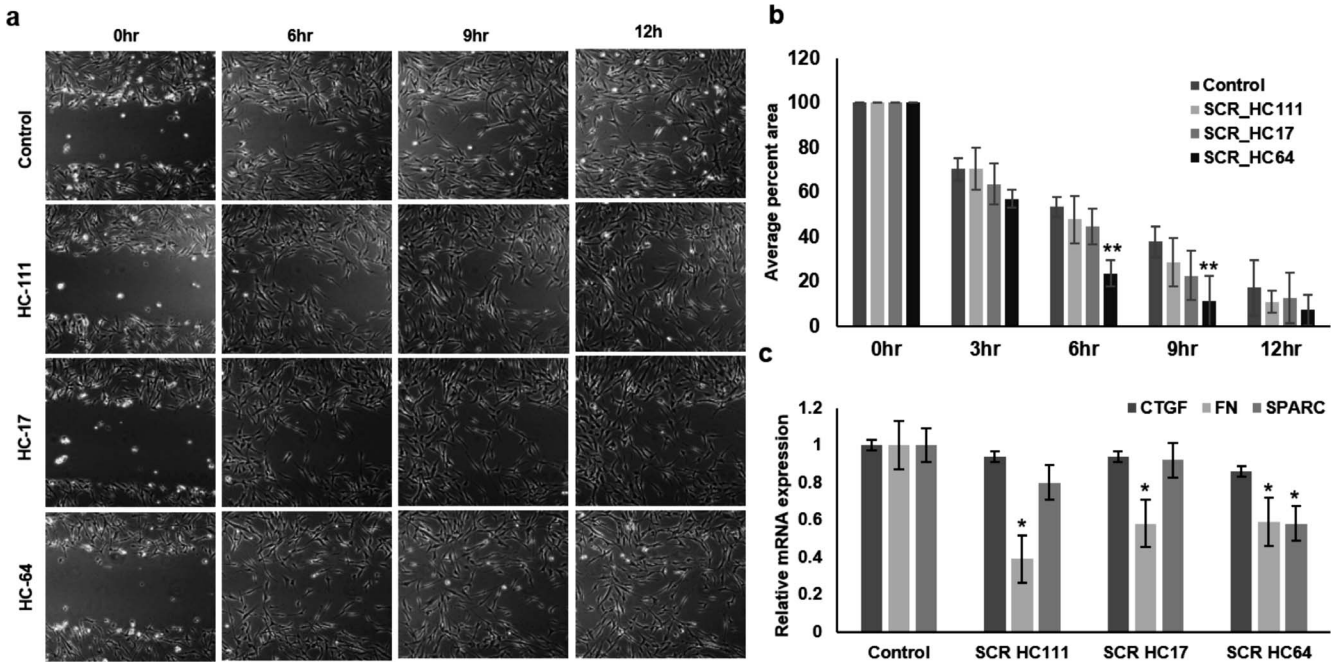

Figure 7. Corneal wound healing by stem cell secretome. (**a**) *Phase-contrast images* for temporal live-cell assessment of effect of secretome obtained from various CSSCs on wound-healing capacity of corneal fibroblasts (magnification ×10). (**b**) *Bar diagram* showing the average percentage area covered by cells in wound after different time intervals. (**c**) qPCR analysis for fibrotic markers in corneal fibroblasts at control and post secretome treatment level. $^{*}P < 0.05$, $^{**}P < 0.001$, $^{***}P < 0.0001$.

Investigative Ophthalmology & Visual Science

years of cryopreservation, which reflects their good candidacy for cell therapy–based applications after long-term cryopreservation. The maintenance of colony formation and spheroid-forming tendency in these cells post thaw indicates that these can rapidly proliferate in culture and single cell still maintained their potency to give rise to daughter cells.

Our group at the University of Pittsburgh reported for the first time, the existence of CSSCs near the corneal limbus.[15] We reported the multipotent nature of CSSCs in the study demonstrating their directed differentiation into chondrocytes, keratocytes, and glial fibrillary acidic protein/NF-expressing neurons. There is no extensive literature available about the differentiation of these cells into cells of different lineages. Hashmani et al.[34] demonstrated the osteogenic and chondrogenic differentiation capacity of peripheral and limbal corneal stromal cells when cultured under specific induction media. The directed differentiation of all three cryo-CSSCs to osteocytes in our study after such a long-term storage indicated that these cells can be used for bone-related disorders in the long run. However, the lower osteogenic potential of HC111 as compared with HC17 and HC64 indicated that there can be patient-specific variations into differentiation capacity of stem cells over time. D'Ippolito and colleagues[35] reported that the osteogenic potential of MSCs decreases with increased age in humans, which might account for age-related osteoporosis and other bone-related complications. The lower osteogenic potential of HC111 hence can be well understood by the fact that these cells were obtained from a donor aged 45 (Supplementary Table S1).[35] Patient-specific variations also may account for the lower adipogenic potential of HC64 as compared with the other two cryo-CSSC populations.

B-III tubulin is an exclusive marker for neurons and is an important component of microtubules. Due to its role in early neural development, it is now well established as a marker for neural differentiation and to distinguish the multipotent nature of stem cells.[36,37] NFs serve as support anchors for neuronal cytoskeleton and help in regulation of axon diameter in neurons.[38] NF can distinctly differentiate neurons (NF+) from glial cells (NF–), and hence serve as an important biomarker for neural differentiation and many neuronal pathological diseases.[39] Use of these two markers helped us to potently characterize the neural differentiation of cryo-CSSCs. Positive expression of these proteins in differentiated populations and negative expression in control undifferentiated cryo-CSSCs indicated that these cells maintained the tendency to make neurons after a prolonged period of cryopreservation. Almost no change in the level of Nestin may be explained by the high expression of Nestin even at baseline by undifferentiated CSSCs. This provides a hope for use of CSSCs in the long run for cell-based therapies for various neurodegenerative disorders, such as Alzheimer's and Parkinson's.

Corneal keratocytes are mesenchymal in origin and derived from neural crest. These cells play an important role in the maintenance of corneal transparency and corneal stroma.[40] After a wound, keratocytes differentiate into fibroblasts or myofibroblasts and corneal scar normally forms during wound healing because of the abnormal ECM secreted by fibroblasts and myofibroblasts. SCT normally works by differentiation of stem cells into cells of resident phenotype as well as providing trophic support to the cells.[41,42] We demonstrated that CSSCs have the ability to secrete a corneal-like tissue during in vitro conditions.[20] Hence, we evaluated the capacity of cryo-CSSCs to differentiate into corneal keratocytes and these differentiated cells were able to secret the important proteoglycans keratocan and keratin sulfate, which are important to maintain corneal transparency. This result indicates the uninhibited use of CSSCs for ocular applications after long-term storage.

Recent burnouts of SCT involved disastrous failure of few clinical trials in which patients observed devastating outcomes and filed lawsuits on the clinics. One of reports published by Kuriyan et al.[43] reported the permanent vision loss in three women with acute macular degeneration who received autologous SCT using adipose tissue–derived stem cells derived from their own fat tissue. This report emphasizes the loopholes for lacking the Good Manufacturing Practices (GMPs) for preparation of cell-based products and also the lack of proper regulations to guide such treatments. To address these issues, The Food and Drug Administration (FDA) recently published their perspective regarding risks and benefits associated with SCT.[44] The FDA authorities urged the design of safer therapies by following proper GMP guidelines as well as designing innovative therapies to complement the already existing therapies. Paradigm is now shifting to a stem "cell-free" therapy in which growth factors/secretome derived from stem cells can be used to impart the therapeutic effect of stem cells without much concern about side effects because the cellular part is bypassed.[45,46] Hence, we tried to delineate the effect of secretome derived from cryo-CSSCs on the wound-healing potential of corneal fibroblasts, which provided encouraging results because the secretome derived from HC64 could significantly promote the wound-healing capacity of fibroblasts. Corneal injury leads to corneal scarring, which results from unregulated deposition of ECM components.[47] SPARC has been reported to be the main mediator of fibrosis, as it does not play any important role in structural organization, but once secreted, it can modulate the interaction between cells and surrounding ECM. An elevated level of SPARC has been found in animal models of many fibrotic diseases involving different tissues, including eyes.[48] Fibronectin has also been reported as a main marker of fibrosis in complications involving liver fibrogenesis and in some forms of GvHD.[49,50] CTGF is also reported to be involved in mediating fibrosis and an important drug target for fibrosis inhibition.[51] In our study, secretome from HC64 could reduce the expression of SPARC and fibronectin, whereas the secretome from HC111 and HC17 could reduce the expression of fibronectin. Furthermore, the increased wound-healing effect of secretome may be related to increased cell migration and proliferation of corneal fibroblasts. It may be worth mentioning that significant increase in wound-healing potential (HC64-patient age 25) and reduction in fibrosis markers (fibronectin and SPARC, HC64-patient age 25) has occurred in young patients, whereas fibronectin was reduced in secretome from all three CSSCs, irrespective of the age of the patient. Hence, secretome from young stem cells might hold more potential for wound healing and reducing fibrosis. However, future studies may help to address this difference in a more profound way. Deep insights into molecular characterization of secretome can lead to the identification of small molecules present in CSSC secretome, which led to the reduced expression of SPARC and fibronectin and promoting wound healing at the same time.

Conclusions

This study urges encouraged application of CSSCs into vast areas of regenerative medicine, such as bone disorders, neurodegeneration, and ocular diseases, even after a long time of storage and stem cell banking. Because CSSCs could be obtained by biopsy, it is possible to use them for autologous purposes. Further, CSSC secretome can also be a potential dual drug candidate for increasing wound-healing capacity of corneal fibroblasts during corneal injury by increasing their regenerative potential and decreasing fibrosis at the same time.

Investigative Ophthalmology & Visual Science

Acknowledgments

The authors thank Nancy Zurowski for help with Flow Cytometry and Kira Lathrop (Imaging Core Module) for help with imaging.

Supported by National Institutes of Health grants EY025643 (YD) and P30-EY008098, Research to Prevent Blindness, Eye and Ear Foundation (Pittsburgh, PA, USA), the National Natural Science Foundation of China (No. 81570817).

Disclosure: **A. Kumar**, None; **Y. Xu**, None; **E. Yang**, None; **Y. Du**, None

References

1. Venkataramana NK, Kumar SK, Balaraju S, et al. Open-labeled study of unilateral autologous bone-marrow-derived mesenchymal stem cell transplantation in Parkinson's disease. *Transl Res*. 2010;155:62–70.
2. Lee HJ, Lee JK, Lee H, et al. The therapeutic potential of human umbilical cord blood-derived mesenchymal stem cells in Alzheimer's disease. *Neurosci Lett*. 2010;481:30–35.
3. Ishibashi S, Sakaguchi M, Kuroiwa T, et al. Human neural stem/progenitor cells, expanded in long-term neurosphere culture, promote functional recovery after focal ischemia in Mongolian gerbils. *J Neurosci Res*. 2004;78:215–223.
4. Lopez-Vales R, Fores J, Verdu E, Navarro X. Acute and delayed transplantation of olfactory ensheathing cells promote partial recovery after complete transection of the spinal cord. *Neurobiol Dis*. 2006;21:57–68.
5. Martin-Rendon E, Brunskill SJ, Hyde CJ, Stanworth SJ, Mathur A, Watt SM. Autologous bone marrow stem cells to treat acute myocardial infarction: a systematic review. *Eur Heart J*. 2008; 29:1807–1818.
6. Ramaesh K, Dhillon B. Ex vivo expansion of corneal limbal epithelial/stem cells for corneal surface reconstruction. *Eur J Ophthalmol*. 2003;13:515–524.
7. Holland EJ, Djalilian AR, Schwartz GS. Management of aniridic keratopathy with keratolimbal allograft: a limbal stem cell transplantation technique. *Ophthalmology*. 2003;110:125–130.
8. Kumar A, Bhattacharyya S, Rattan V. Effect of uncontrolled freezing on biological characteristics of human dental pulp stem cells. *Cell Tissue Bank*. 2015;16:513–522.
9. Yong KW, Wan Safwani WK, Xu F, Wan Abas WA, Choi JR, Pingguan-Murphy B. Cryopreservation of human mesenchymal stem cells for clinical applications: current methods and challenges. *Biopreserv Biobank*. 2015;13:231–239.
10. Moll G, Alm JJ, Davies LC, et al. Do cryopreserved mesenchymal stromal cells display impaired immunomodulatory and therapeutic properties? *Stem Cells*. 2014;32:2430–2442.
11. Francois M, Copland IB, Yuan S, Romieu-Mourez R, Waller EK, Galipeau J. Cryopreserved mesenchymal stromal cells display impaired immunosuppressive properties as a result of heat-shock response and impaired interferon-gamma licensing. *Cytotherapy*. 2012;14:147–152.
12. Luetzkendorf J, Nerger K, Hering J, et al. Cryopreservation does not alter main characteristics of Good Manufacturing Process-grade human multipotent mesenchymal stromal cells including immunomodulating potential and lack of malignant transformation. *Cytotherapy*. 2015;17:186–198.
13. Katayama Y, Yano T, Bessho A, et al. The effects of a simplified method for cryopreservation and thawing procedures on peripheral blood stem cells. *Bone Marrow Transplant*. 1997; 19:283–287.
14. Gramlich OW, Burand AJ, Brown AJ, Deutsch RJ, Kuehn MH, Ankrum JA. Cryopreserved mesenchymal stromal cells maintain potency in a retinal ischemia/reperfusion injury model: toward an off-the-shelf therapy. *Sci Rep*. 2016;6:26463.
15. Du Y, Funderburgh ML, Mann MM, SundarRaj N, Funderburgh JL. Multipotent stem cells in human corneal stroma. *Stem Cells*. 2005;23:1266–1275.
16. Basu S, Hertsenberg AJ, Funderburgh ML, et al. Human limbal biopsy-derived stromal stem cells prevent corneal scarring. *Sci Transl Med*. 2014;6:266ra172.
17. Hertsenberg AJ, Shojaati G, Funderburgh ML, Mann MM, Du Y, Funderburgh JL. Corneal stromal stem cells reduce corneal scarring by mediating neutrophil infiltration after wounding. *PLoS One*. 2017;12:e0171712.
18. Du Y, Carlson EC, Funderburgh ML, et al. Stem cell therapy restores transparency to defective murine corneas. *Stem Cells*. 2009;27:1635–1642.
19. Wu J, Du Y, Mann MM, Funderburgh JL, Wagner WR. Corneal stromal stem cells versus corneal fibroblasts in generating structurally appropriate corneal stromal tissue. *Exp Eye Res*. 2014;120:71–81.
20. Du Y, Sundarraj N, Funderburgh ML, Harvey SA, Birk DE, Funderburgh JL. Secretion and organization of a cornea-like tissue in vitro by stem cells from human corneal stroma. *Invest Ophthalmol Vis Sci*. 2007;48:5038–5045.
21. Wu J, Du Y, Mann MM, Yang E, Funderburgh JL, Wagner WR. Bioengineering organized, multilamellar human corneal stromal tissue by growth factor supplementation on highly aligned synthetic substrates. *Tissue Eng Part A*. 2013;19:2063–2075.
22. Wu J, Du Y, Watkins SC, Funderburgh JL, Wagner WR. The engineering of organized human corneal tissue through the spatial guidance of corneal stromal stem cells. *Biomaterials*. 2012;33:1343–1352.
23. Syed-Picard FN, Du Y, Hertsenberg AJ, et al. Scaffold-free tissue engineering of functional corneal stromal tissue. *J Tissue Eng Regen Med*. 2016;12:59–69.
24. Funderburgh JL, Funderburgh ML, Du Y. Stem cells in the limbal stroma. *Ocul Surf*. 2016;14:113–120.
25. Frade JM, Bovolenta P, Rodriguez-Tebar A. Neurotrophins and other growth factors in the generation of retinal neurons. *Microsc Res Tech*. 1999;45:243–251.
26. Chimenti I, Smith RR, Li TS, et al. Relative roles of direct regeneration versus paracrine effects of human cardiosphere-derived cells transplanted into infarcted mice. *Circ Res*. 2010; 106:971–980.
27. Chen L, Tredget EE, Wu PY, Wu Y. Paracrine factors of mesenchymal stem cells recruit macrophages and endothelial lineage cells and enhance wound healing. *PLoS One*. 2008;3: e1886.
28. Kim DK, Nishida H, An SY, Shetty AK, Bartosh TJ, Prockop DJ. Chromatographically isolated CD63+CD81+ extracellular vesicles from mesenchymal stromal cells rescue cognitive impairments after TBI. *Proc Natl Acad Sci U S A*. 2016;113:170–175.
29. Raik S, Kumar A, Bhattacharyya S. Insights into cell-free therapeutic approach: role of stem cell "soup-ernatant." *Biotechnol Appl Biochem*. 2017;65:104–118.
30. Kumar A, Kumar V, Rattan V, Jha V, Pal A, Bhattacharyya S. Molecular spectrum of secretome regulates the relative hepatogenic potential of mesenchymal stem cells from bone marrow and dental tissue. *Sci Rep*. 2017;7:15015.
31. Kumar A, Kumar V, Rattan V, Jha V, Bhattacharyya S. Secretome cues modulate the neurogenic potential of bone marrow and dental stem cells. *Mol Neurobiol*. 2017;54:4672–4682.
32. Friedlander M. Fibrosis and diseases of the eye. *J Clin Invest*. 2007;117:576–586.
33. Iosfina I, Chuo JY, Godinho DV, Wilcox PG, Kreisman SH, Quon BS. Optic disc swelling and vision loss in a patient with cystic fibrosis and diabetes. *Case Rep Endocrinol*. 2013;2013:843795.
34. Hashmani K, Branch MJ, Sidney LE, et al. Characterization of corneal stromal stem cells with the potential for epithelial transdifferentiation. *Stem Cell Res Ther*. 2013;4:75.

35. D'Ippolito G, Schiller PC, Ricordi C, Roos BA, Howard GA. Age-related osteogenic potential of mesenchymal stromal stem cells from human vertebral bone marrow. *J Bone Miner Res*. 1999;14:1115–1122.
36. Katsetos CD, Del Valle L, Geddes JF, et al. Aberrant localization of the neuronal class III beta-tubulin in astrocytomas. *Arch Pathol Lab Med*. 2001;125:613–624.
37. Sieber-Blum M, Schnell L, Grim M, Hu YF, Schneider R, Schwab ME. Characterization of epidermal neural crest stem cell (EPI-NCSC) grafts in the lesioned spinal cord. *Mol Cell Neurosci*. 2006;32:67–81.
38. Lohrke S, Brandstatter JH, Boycott BB, Peichl L. Expression of neurofilament proteins by horizontal cells in the rabbit retina varies with retinal location. *J Neurocytol* 1995;24:283–300.
39. Rosengren LE, Karlsson JE, Karlsson JO, Persson LI, Wikkelso C. Patients with amyotrophic lateral sclerosis and other neurodegenerative diseases have increased levels of neurofilament protein in CSF. *J Neurochem*. 1996;67:2013–2018.
40. Pinnamaneni N, Funderburgh JL. Concise review: stem cells in the corneal stroma. *Stem Cells*. 2012;30:1059–1063.
41. Rennert RC, Sorkin M, Garg RK, Gurtner GC. Stem cell recruitment after injury: lessons for regenerative medicine. *Regen Med*. 2012;7:833–850.
42. Rustad KC, Gurtner GC. Mesenchymal stem cells home to sites of injury and inflammation. *Adv Wound Care (New Rochelle)*. 2012;1:147–152.
43. Kuriyan AE, Albini TA, Townsend JH, et al. Vision loss after intravitreal injection of autologous "stem cells" for AMD. *N Engl J Med*. 2017;376:1047–1053.
44. Marks PW, Witten CM, Califf RM. Clarifying stem-cell therapy's benefits and risks. *N Engl J Med*. 2017;376:1007–1009.
45. Furuta T, Miyaki S, Ishitobi H, et al. Mesenchymal stem cell-derived exosomes promote fracture healing in a mouse model. *Stem Cells Transl Med*. 2016;5:1620–1630.
46. Phinney DG, Pittenger MF. Concise review: MSC-derived exosomes for cell-free therapy. *Stem Cells*. 2017;35:851–858.
47. Torricelli AA, Santhanam A, Wu J, Singh V, Wilson SE. The corneal fibrosis response to epithelial-stromal injury. *Exp Eye Res*. 2016;142:110–118.
48. Trombetta-Esilva J, Bradshaw AD. The Function of SPARC as a mediator of fibrosis. *Open Rheumatol J*. 2012;6:146–155.
49. Liu XY, Liu RX, Hou F, et al. Fibronectin expression is critical for liver fibrogenesis in vivo and in vitro. *Mol Med Rep*. 2016;14:3669–3675.
50. van der Straaten HM, Canninga-van Dijk MR, Verdonck LF, et al. Extra-domain-A fibronectin: a new marker of fibrosis in cutaneous graft-versus-host disease. *J Invest Dermatol*. 2004;123:1057–1062.
51. Lipson KE, Wong C, Teng Y, Spong S. CTGF is a central mediator of tissue remodeling and fibrosis and its inhibition can reverse the process of fibrosis. *Fibrogenesis Tissue Repair*. 2012;5:S24.

Investigative Ophthalmology & Visual Science